INTERNATIONAL JOURNAL OF TECHNO-ENGINEERING
IJTE

ISSN: 2057-5688

Brain Tissue Segmentation Employing an Enhanced Kernelized Rough-Fuzzy C-Means Method

Mr. Parveen Kumar

Assistant Professor, Govt College Hisar

Abstract: An active and difficult topic of biomedical engineering and machine learning is the analysis of MRI scans of the brain. Radiologists and other medical professionals cannot effectively recommend or implement therapy without first identifying and localising anomalies, such as tumours, edoema, and so on. Besides being one of the most popular diagnostic imaging methods, MRI's other benefits include being able to produce detailed multimodal scans of different tissues of the human brain with varying contrast using the three magnetic resonance modalities (T1 weighted, T2 weighted, and T3 weighted). However, Brain MRI may be affected by noise, outliers, and other anomalies. Due to the potential existence of noise and outliers in brain MRI, traditional unsupervised machine learning algorithms generally fail to yield correct segmentation results. White matter (WM), grey matter (GM), cerebrospinal fluid (CSF), etc. are all parts of the brain, and their boundaries are sometimes hazy and difficult to nail down. Different tissues can't be isolated in a linear fashion, either. In light of these problems, this thesis makes an effort to tackle issues like (i) noise in brain MRI datasets; (ii) ambiguity in defining brain tissue regions; (iii) non-linear separation of different brain tissue regions; and (iv) inaccuracy in the performance of traditional unsupervised methods. By skillfully combining (a) the use of a kernel technique increases the likelihood of distinct brain tissue areas being linearly separable in its original feature space, even if they would not have been otherwise, the present thesis proposes some robust and novel unsupervised, semi-supervised, and ensemble learning techniques. By providing some labelled pixels with a constraint-seeded policy, we use spatial contextual information (b), a fuzzy set (c), a rough set (d), and finally a fuzzy set (e) to guide the clustering process in better direction, allowing it to better deal with likely noise, outliers, and other artefacts. In addition, a collection of unsupervised algorithms is used to arrive at a judgement.

INTERNATIONAL JOURNAL OF TECHNO-ENGINEERING
IJTE
ISSN: 2057-5688

I. Introduction

The human brain is the most intricate organ, since it is responsible for regulating every aspect of the body by processing information received from the environment [1-4]. The brain is responsible for numerous functions [3, 4], including memory, intellect, emotion, and creativity. The skull serves as primary protection for the brain's primary components—the cerebrum, cerebellum, and brainstem. Cerebrum: The cerebrum takes up most of the human brain's real estate. In Figure 1, we see the left and right hemispheres of the cerebrum. The cerebrum is responsible for the majority of the body's processes [2, 3], including sight, hearing, interpretation, learning, emotion, logic, and communication. The cerebellum is a small brainstem that sits at the base of the brain. The cerebellum's primary roles are in motor control and equilibrium. The brainstem is a hub of communication between the brain and spinal cord, processing signals from the cerebellum and the cerebral cortex. The brainstem is responsible for maintaining homeostasis, or the maintenance of major routine functions such as waking, sleep, body temperature, heart rate, breathing, coughing, sneezing, digesting, and vomiting. [1–4].

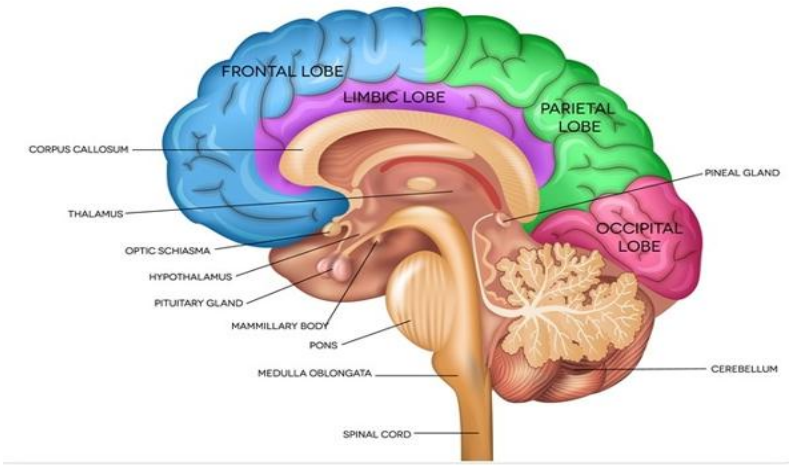

Figure 1.1: Anatomy of human Brain

The outer layer of the brain, called the cortex, [2]. It has valleys and hills and is folded in shape, and it contains around 16 billion neurons that are laid out in certain layers [3]. A typical picture of the cerebral cortex is shown in Figure 1.3 [3]. A gyrus is a ridge in the brain, while a sulcus is a depression between ridges [1,4]. The term "grey matter" (GM) describes

ISSN: 2057-5688

the cell bodies that give the cortex its characteristic greyish brown colour. Long nerve cells called white matters (WM) connect the various regions of the brain [1-4]. The CSF is a transparent fluid that continually moves through the brain and spinal cord. The cerebrospinal fluid (CSF) carries glucose, oxygen, and other chemicals from the blood and serves the fundamental function of protecting the human brain from physical and chemical harm [1, 5, 6]. The WM is the principal pathway for signals to go between the left and right hemispheres of the cerebral cortex [1,4,5]. Learning, language, memory, and conscious awareness are all under the GM's control [1, 4].

The coronal plane, also known as the frontal plane, splits the brain horizontally.

A sagittal plane perpendicular to the coronal plane divides the brain vertically into two hemispheres.

Perspective: horizontal or vertical? The axial plane, transverse plane, or horizontal plane divides the brain into inferior and superior hemispheres perpendicular to the sagittal and coronal planes. Stand a brain on end and its axial plane will be perpendicular to the floor. Cutting a surface at an angle creates cross sections [1, 3, 4].

The brain may develop several illnesses. Common human brain abnormalities are covered here.

Uncontrolled brain cell proliferation causes brain tumours [7, 8]. Many forms of brain tumours are malignant. Malignant tumours, the most dangerous kind of cancer, may spread to the brain. Since primary brain tumours don't metastasize, benign tumours are safer [7-9]. The four main brain tumour severity ratings are I–IV [7, 10]. Under a microscope, grade I brain tumour cells seem normal and grow slowly. They have the lowest chance of spreading malignancy and the best prognosis. Grade I brain tumours may benefit from surgery. Grade I brain tumours include gangliocytoma and ganglioglioma [10]. Grade II brain tumours grow slowly, contain abnormal cells, and may spread. A malignant grade III brain tumour divides rapidly and may quickly become a grade IV tumour. Anaplastic astrocytoma is a grade III brain tumour. The most malignant brain tumours are grade IV. Grade IV tumours have necrotic cells at their core. This cancer grows quickly, invades adjacent cells, and requires

ISSN: 2057-5688

new blood arteries to grow. A grade IV brain tumour is glioblastoma, sometimes called malignant astrocytic glioma [7-9].

Alzheimer's disease (AD) often causes dementia, which impairs fundamental cognitive processes including remembering, thinking, and reasoning. AD is a progressive, irreversible neurodegenerative condition that kills brain cells and cognitive function, causing dementia [11, 12]. Inability to recall recent conversations or experiences may indicate Alzheimer's disease. Alzheimer's disease causes memory loss, difficulty to perform everyday tasks, and death [7, 13] owing to brain function decline. Alzheimer's often hits in the early 60s.

Parkinson's disease (PD), a degenerative brain illness, causes shaking/trembling, trouble walking, movement dysfunction, and loss of coordination. Neurodegeneration worsens the illness [7]. In their late 50s, PD symptoms include hand, foot, and facial tremors, sluggish mobility, and balance and coordination issues. US prevalence of PD is second only to Alzheimer's [13].

A short disruption in cerebral blood flow or severe brain haemorrhage may induce stroke [17, 18]. After a stroke, one may have trouble walking, talking, understanding, sensation in their arms, legs, or face, or even paralysis [17]. The most frequent strokes are ischemic and hemorrhagic. Ischemic strokes are caused by a shortage of blood flow, whereas hemorrhagic strokes are caused by brain haemorrhage [18]. Early therapy may slow brain cell damage and prevent strokes.

II. Literature Survey

Computer tomography (CT), x-ray photography, positron emission tomography (PET), and magnetic resonance imaging (MRI) are all examples of diagnostic imaging technologies used in the medical field. Among the various medical imaging methods, magnetic resonance imaging (MRI) may be the most useful and vital for the early diagnosis of pathological abnormalities in tissues and organs. Imaging the brain is one of MRI's most important applications. In this risk-free and noninvasive treatment, images of the brain and brain stem are obtained by subjecting the patient to a magnetic field and radio waves. Multimodal imaging of tissues with varying contrasts may be created using T1 weighted, T2 weighted, and PD (proton density) weighted MRI images [19, 28, 31]. The complex anatomy of the

ISSN: 2057-5688

brain makes accurate segmentation crucial for detecting tumours, edoema, necrotic tissues, and other abnormalities. Chemical, anatomical, and morphological tests in clinical settings were traditionally used to identify these variations.

Sanghamitra In a 2015 study led by T. Kamble et al., cell samples from the encephalon were extracted using the K-means approach to reveal many types of cancer. The "k-means" technique and tumours need a noise-free image as an input.

Researchers Malathi R. et al. Segmentation plays a crucial function in the dissemination of medical images by deleting potentially problematic parts of the photos. They proposed a K-Means clustering-based method for segmenting MRI scans of the brain in order to locate tumours.

A. Santhosh rishnan, G. Santhosh rishnan, et al. The median filter, GLCM, fuzzy c-means, artificial neural fuzzy skill, and ANFIS are all used in this image analysis to minimise noise, divide the pictures, and classify brain tumours, respectively. Brain tumour types and other abnormalities were determined by analysing MRI scans. Several image pre-processing methods are used to medical images, after which partitioning is used to isolate tumours from the rest of a brain image, and finally, feature extraction strategies are investigated.

The implementation of medical picture inquiry may be considerably improved by the inclusion of an evaluation set of rules with a variety of investigative and diagnostic conditions (Zhongyu Li et al., 2017). Using a "SVM Classifier" and segmentation, T. Sathies Kumar and colleagues (2017) developed a method for detecting tumours in the encephalon. This method uses MRI slices to contain a mass of abnormal cells, and then trains an artificial neural network to identify the type of tumour based on features extracted from the segmented area.

In 2017, Emre Dandi and coworkers This is why graphical user interfaces (GUIs) have been developed for computer programmes. Therefore, the culpable physicians' cases will be revealed. As a result, the programme will be more accurate and might one day be used to enhance traditional methods of segmenting brain tumours. Extensive testing using image datasets has shown the app's ability to accurately identify brain tumours.

III. Proposed Methodology

ISSN: 2057-5688

Biomedical engineers possess a deep understanding and appreciation for the immense significance that imaging technologies hold in the realm of clinical diagnosis. Numerous diagnostic instruments are present in the domain of medical imaging technology. A plethora of imaging modalities are at one's disposal, encompassing X-ray radiography, computed tomography (CT), magnetic resonance imaging (MRI), and positron emission tomography (PET) scans. Magnetic resonance imaging (MRI) stands as a widely favoured and highly efficacious diagnostic imaging technique that possesses the capability to detect subtle alterations within organs and tissues during their nascent phases. Magnetic resonance imaging (MRI) is a widely employed and highly esteemed diagnostic modality due to its ability to generate exceptional visual representations of the brain and its substructures through the utilisation of a magnetic field and radio waves. Brain MRIs, which are frequently employed within the realm of medical diagnostics, serve as a common modality for the examination and evaluation of neurological conditions. In the realm of brain MRI, the utilisation of T1, T2, and PD (proton density) weighted methodologies can be employed to furnish multimodal representations of tissues exhibiting divergent contrasts.

Augmented spatial framework The process of kernelization involves the transformation of a problem into a more simplified and compact form The process of dividing brain tissue into distinct segments Employing the concept of Rough Fuzzy The C-Means algorithm is a computational method used for cluster analysis and data clustering.

The incorporation of rough-fuzzy clustering entailed the utilisation of the kernel-trick principle, which was subsequently subjected to alterations and enhancements through the integration of spatial constraints. This action was undertaken in order to attend to the inquiries that were raised in the introductory section (pertaining to contextual particulars). The anticipated outcome of this technique is to deliver accurate partitioning, specifically for intricate cerebral (MRI) tissue divisions that exhibit uncertainty, convergence, arduous differentiation in their original state, and occasionally contaminated by interference.

By employing the kernel method, it becomes feasible to transform the data pattern (pixels) xk and the cluster centre (vi) into a space of higher dimensions. The likelihood of cluster dispersal in this space is higher compared to the previous one, primarily due to the presence of a linear barrier. The utilisation of the kernel method involves the application of a Mercer

ISSN: 2057-5688

kernel in order to execute a non-linear transformation on the input data points. To effectively perceive and comprehend the information contained within a feature space that possesses numerous dimensions, this task is undertaken. Due to the inherent complexity of these regions, their linear separability in the original feature space is limited. However, the utilisation of a kernel approach enhances the probability of achieving separation through the application of a linear metric.

A tiny window (usually 33 or 55) is used to indicate the mean or median of the near adjacent pixels (i.e., those that are present in a short window around the pixel of interest). Two parts of Equation (3.5) are involved, with the first part being directly associated with and borrowed from the standard Fuzzy C-Means (FCM) types algorithm with kernel, and the second part being in charge of computing the mean or median of the immediate neighbouring pixels around any given pixel xk, which aids in dealing with noise or outliers present in the image and is intended to improve performance of the segmentation method. The mean filtering or median filtering approach (in this case, the mean value for x e k) may be used to calculate x e k in advance, as opposed to [97], and the controlling parameter, which governs the influence of the surrounding term, is utilised in the current study. In cases This method is identical to standard KFCM when either or is zero or infinite.

Algorithm: Kernelized Rough − Fuzzy

Input: Set of pixels $\vec{x}_k$ present in the image, number of clusters C, and user defined parameters $(m, \alpha$, threshold, and $w_{low})$.

Output: Set of segmented pixels (in the form segmented image).

Method:

1: Mean vector $\vec{x}_k(\forall k)$ is computed in advance for the neighbouring pixels within a small window centering around $\vec{x}_k$.

2: Cluster centers $\vec{v}_i, \forall i = 1$ to C are assigned randomly in the initial stage.

3: while (not convergence) do

4: Memberships μ_{ik} is computed by using Equation (3.6) for all clusters C and all pixels N.

5: for each pixel $\vec{x}_k, k = 1: N$ do

6: Assign the maximum membership grade for pixel $\vec{x}_k$ as follows:

ISSN: 2057-5688

$$\mu_{pk} \leftarrow \max_{j=1:C}(\mu_{jk}),$$

where, $p = \text{argmax}$

7: for $j = 1:C$ and $j \neq p$ do

8: if $\mu_{jk}/\mu_{pk} >$ threshold then

9: $\vec{x}_k$ is assigned to the upper approximations $\bar{B}X_j$ and $\bar{B}X_p$.

10: end if

11: end for

12: if $\vec{x}_k \notin$ any upper approximation then

13: if $\vec{x}_k \notin$

14: $\vec{x}_k$ is
end if

15: end for

16: Cluster centers $\vec{v}_i, \forall i = 1:C$ are updated based on Equation (3.13).

17: end while

The basis of MRI segmentation is partitive clustering, which requires iteratively assigning pixels to the potential clusters until convergence is attained. We claim that the clustering process has converged when there are no longer any discernible changes in cluster centres between two consecutive rounds of (re)assigning pixels. The well-known Gauss-Seidel algorithm [48] may be used to bring the suggested technique to convergence. If there are only diagonally dominating equations in the confusion matrix (CM), then the Gauss-Seidel technique will converge. Equations based on confusion matrices (CMs) are utilised to describe the process. Confusion matrix Mcc of dimension C x C (where C is the number of clusters) may be generated based on pixels allocated to each cluster at each step of the operation. If the CM is diagonally dominating, then the clustering process is said to have converged; otherwise, convergence is considered possible but unlikely. Each row of the CM must have a cardinality greater than zero for it to converge, and the cardinality of the off-diagonal components in that row must be zero or less than the cardinality of the diagonal elements in that row.

IV. Experimental Evaluation

3.4.1 MRI datasets used

ISSN: 2057-5688

Experiments are conducted on a variety of datasets from the BrainWeb image collection and the IBSR image database, as well as generated benchmark MRI datasets with and without noise. BrainWeb is an artificial intelligence system, in contrast to the real-world IBSR dataset. White matter (WM), grey matter (GM), cerebrospinal fluid (CSF), and background clusters are thought to be part of every MRI scan of the brain for determining which areas are most crucial. Images in the BrainWeb dataset are (217 x 181) in size, whereas the same image in the IBSR dataset is (128 x 256). T1 and T2 weighted modalities are being investigated for these objectives. Examples of common MRI data sets are shown in Figure 3.1 for the Z85, Z93, Z95, and Z100 planes in T1 and T2 weighted modalities, and for the Z93, Z95, and Z100 planes in T2 weighted modalities. Typical Z85 ground-truth images are shown as examples in Figure 3.2. By taking into account the principal brain portion (i.e., white matter (WM), grey matter (GM), and CSF) and assigning the pixel in the appropriate segment for which the largest degree of fuzzy membership is determined, the database provides fuzzy ground facts for each segment. Images with no white matter demonstrate the absence of additional smaller brain areas. Additionally, the ground realities for many common IBSR datasets (including IBSR144, IBSR150, IBSR155, and IBSR167) are provided.

Coefficient of Jaccard

The intersection (IOU) coefficient (M) is the fraction of pixels in both the original (L) and segmented (M) pictures that are identical to those in the unified function (or the collection of pixels shared by input (L) and segmented (M) images). Therefore, the Jaccard coefficient (J) is the ratio of the intersection and union of these two values (M), and the summation function (S) reflects the intersection of the pixel values in the input picture (L) and the segmented image (M).

$$J(L, M) = \frac{S(L \cap M)}{S(L \cup M)}$$

The better the segmentation, the higher the value of the Jaccard coefficient. The Jaccard coefficient has a range of 0 to 1, with a maximum of 1. The closer the value of Jaccard comes to one, the better the performance.

Dice coefficient (DC)

ISSN: 2057-5688

Dice coefficient value is stated using the Jaccard index J. (L, M). DC is a function that can be written as where L is the input image and M is the segmented output image:

$$D(L, M) = 2 \times \frac{J(L, M)}{1 + J(L, M)}$$

The highest value of the Dice coefficient is 1, with the range being from 0 to 1. The closer the value of Dice is to one, the better the segmentation.

Kernelized Xie-Beni Index (KXBI)

It's an unsupervised measure for measuring cluster validity. Each cluster's intra-cluster compactness is measured by calculating the average square distance between each pixel and the cluster's centre, while the inter-cluster separation is the lowest square distance between the clusters' centres (or clusters). A lower KXBI number indicates a better-quality cluster. The KXBI may take on values between 0 and 1, with 1 being its maximum. For those interested, the Xie-Beni index after kernelization is defined as:

$$KXBI = \frac{2 \times \sum_{k=1}^{n} \left\{ \sum_{j=1}^{c} \left(1 - \mathbb{K}(\vec{x}_k, \vec{v}_j)^{\frac{1}{1-m}} \right)^{(1-m)} \right\}}{n \times \min_{i \neq j} \left[2 \times \{ 1 - \mathbb{K}(\vec{v}_i, \vec{v}_j) \} \right]}$$

The better the segmentation, the lower the value of the kernelized Xie-Beni index is set to be. The kernelized Xie-Beni index has a range of 0 to 1, with a maximum value of 1.

Finally, in Figure 3.10, ground truths and segmented outputs of the proposed method SEKRFC are summarised, together with a comparison to the other equivalent clustering-based algorithms, for a brain MRI Z100 plane contaminated with 6% "salt and pepper" noise. Typical results of individual segmented images for different regions are also presented in separate figures. Figure 3.10 shows that the recommended SEKRFC method is the only one that can accurately recognise all of the individual segments with either very little or no background noise. On the other hand, despite its critical importance, grey matter cannot be consistently identified using any of the other investigated methods. The results of the experiments were found to be consistent with those of previous MRI scans of the brain. For the full brain MRI dataset, the proposed SEKRFC approach yields much superior

ISSN: 2057-5688

segmentation results than previous clustering-based segmentation methods. This is evident from the validity indices and the clarity with which the segmented pictures may be seen. When it comes to segmenting images that have been altered by "salt and pepper" and "Rician" noises, among other things, the proposed approach surpasses previous similar techniques.

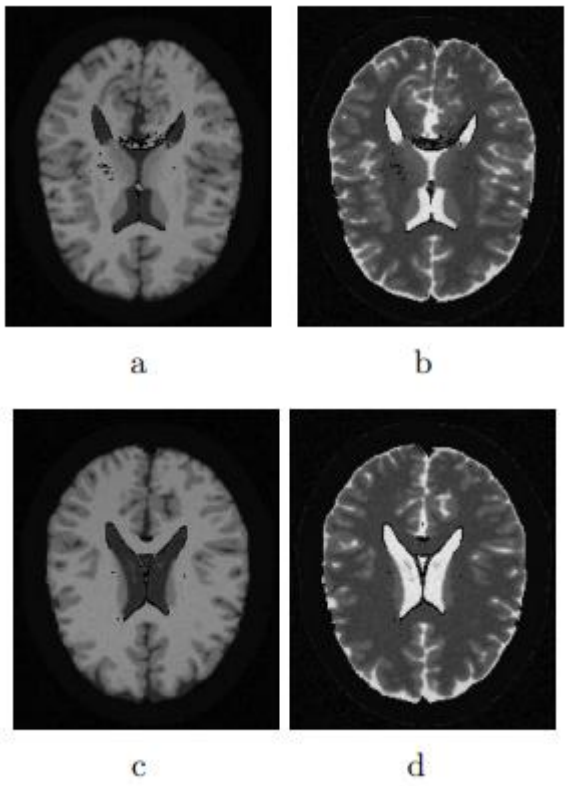

ISSN: 2057-5688

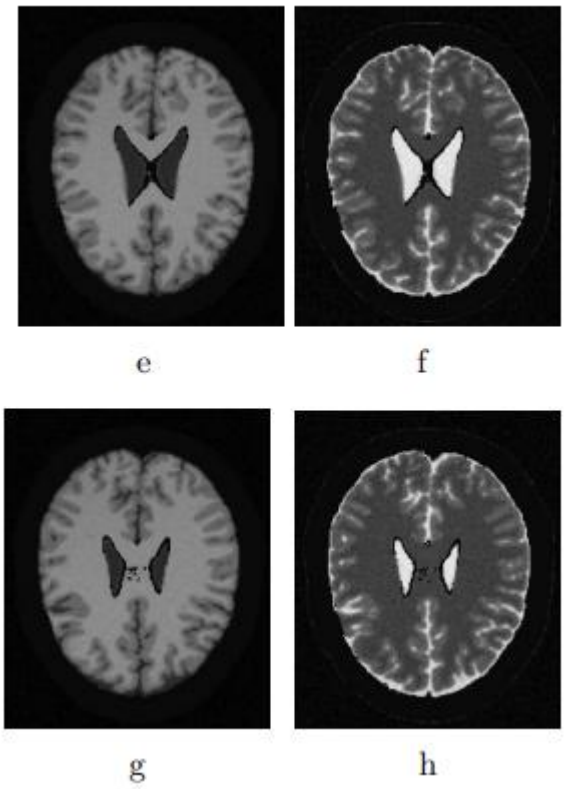

Figure 3.1: In the top row, we have a T1-weighted picture (a) and a T2-weighted image (b) of the brain taken in the Z85 plane, respectively). Second row displays T1- and T2-weighted pictures of the brain in the Z93 plane. In the third row, (e) T1-weighted photos (f) T2-weighted images from a brain MRI taken in the Z96 plane are shown. The fourth row displays the T1- and T2-weighted MRI of the brain in the Z100 plane.

Table 3.6: A brief summary of the recommended method's execution time in seconds

MRI Data	Method						
	FCM	FCMSC	RFCM	KRFCM	KSSCM	RFCMSC	SEKRFC
Z85	70.12	72.20	76.24	80.50	87.10	80.31	87.09
Z93	69.20	73.24	78.22	81.08	89.16	81.11	90.04
Z96	67.26	70.18	72.48	79.08	85.08	80.07	82.42
Z100	69.10	71.22	74.34	79.02	88.20	79.17	90.08

ISSN: 2057-5688

IBSR144	74.02	76.12	79.24	80.16	86.14	82.12	84.08
IBSR150	71.08	72.03	76.18	79.11	84.08	81.28	84.10
IBSR155	69.55	71.20	74.18	77.30	82.32	80.61	83.24
IBSR167	73.16	74.22	77.08	83.14	88.24	84.31	87.20

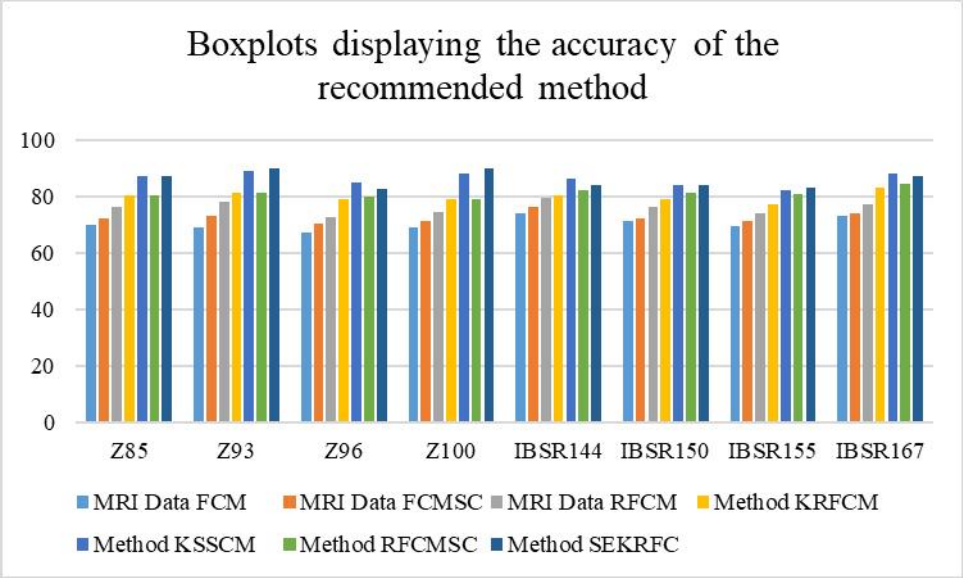

Figure Boxplots displaying the accuracy of the recommended method

According to the experimental findings, the suggested technique (with the exception of the KSSCM method in certain circumstances) requires somewhat more execution time than the other methods under consideration. The proposed approach takes a little more time to execute than current techniques due to the usage of the kernel function and the notion of spatial limits from the neighbouring pixels in the clustering process. When compared to traditional methods of MRI brain tissue segmentation, the suggested method obtained much greater accuracy at the expense of a little increase in execution time.

V. Conclusion

MRI brain tissue segmentation aids in early problem detection. Because brain MRI tissues have ambiguous, fuzzy borders, and overlap, they are notoriously difficult to segment. Tissue bits cannot be separated into straight sections either. Accurate segmentation may also be

ISSN: 2057-5688

hampered by noise in brain MRIs. Expanding on the concept of RFCMSC introduced in Chapter 2, Chapter 3 offers a resilient kernelized rough fuzzy C-means clustering with spatial constraints (KRFCMSC) for brain tissue segmentation from MRI. This is achieved by adding the kernel trick to solve the non-linear separability difficulties of brain tissue areas. In order to address the ambiguity, indiscernibility, vagueness, and overlap of brain tissue areas in brain MRIs, the rough and fuzzy set is recommended for clustering. In brain tissue areas with nonlinear separability, the kernel technique improves linear separability by projecting pixels into higher dimensions. In order to include contextual information and minimise noise and outliers, the clustering approach makes use of geographic boundaries. Real and artificial BrainWeb benchmark brain MRI datasets have been used in noise-free and noise-containing experiments. Segmentation results are assessed using supervised and unsupervised performance validation measures, such as segmentation accuracy (SA), recall, precision, F1 measure (micro and macro averages), Jaccard, dice, Kappa, and kernelized Xie-Beni index. A comparison is made between the suggested brain tissue segmentation technique and FCM, RFCM, FCMSC, KRFCM, and KSSCM. Experiments on MRI brain tissue segmentation demonstrate the superiority and increased resilience of the proposed technology over earlier approaches. The suggested strategy performs better than other approaches, as shown by the t-test and Boxplots.

VI. References

[1] M. C. Wittrock. The Brain and Psychology. Elsevier, Academic Press, United States, first edition, 1980.

[2] T. W. Vanderah and D. J. Gould. Nolte's The Human Brain: An Introduction to its Functional Anatomy. Elsevier, United States, seventh edition, 2015.

[3] Mayfield Education & Research Foundation. Anatomy of the brain. http: //www.mayfieldclinic.com/pe-anatbrain.htm. Accessed: 24 March 2020.

ISSN: 2057-5688

[4] L. M. Biga, S. Dawson, A. Harwell, R. Hopkins, J. Kaufmann, M. LeMaster, P. Matern, K.M. Graham, D. Quick, and J. Runyeon. Anatomy & physiology. https://openstax.org/details/books/ anatomy-and-physiology. Accessed: 24 March 2020.

[5] W. B. Saunders. Basic Human Anatomy. Dartmouth Medical School and Dartmouth College, United States, 1983.

[6] Johnson & Johnson Institute. Anatomy & physiology of the brain. https://jnjinstitute.com/sites/default/files/2019-03/092892-181219-Anatomy-Physiology-of-the-Brain.pdf. Accessed: 24 March 2020.

[7] N. P. Alazraki, M. J. Shumate, and D. A. Kooby. A Clinicians Guide to Nuclear Oncology. Society of Nuclear Medicine and Molecular Imaging, Reston, first edition, 2007.

[8] U. S. Department of Health National Cancer Institute and Human Services. Brain tumor. https://www.cancer.gov/types/brain. Accessed: 24 March 2020.

[9] Mayo Foundation for Medical Education Mayo Clinic and Research (MFMER). Brain tumor. https://www.mayoclinic. org/diseases-conditions/brain-tumor/symptoms-causes/ syc-20350084. Accessed: 24 March 2020.

[10] B. W. Stewart and C. P. Wild. World Cancer Report, chapter Tumours of the nervous systems. World Health Organization, 2014.

[11] Alzheimer's Association. Basics of alzheimer's disease. Technical report, Chicago. https://www.alz.org/alzheimer s dementia.

[12] Prasadu Peddi (2016), Comparative study on cloud optimized resource and prediction using machine learning algorithm, ISSN: 2455-6300, volume 1, issue 3, pp: 88-94.

[13] U.S. Department of Health Nationa Institute of Aging and Human Services. Alzheimer's disease & related dementias. https://www.nia.nih. gov/health/alzheimers/basics. Accessed: 24 March 2020.

[14] L. V. Kalia and A. E. Lang. Parkinson's disease. The Lancet, 386(9996):896–912, 2015.

INTERNATIONAL JOURNAL OF TECHNO-ENGINEERING
IJTE
ISSN: 2057-5688